Available online at www.sciencedirect.com

ScienceDirect

Materials Today: Proceedings 8 (2019) 696–705

materialstoday: PROCEEDINGS

www.materialstoday.com/proceedings

ECT_2017

Long term stability testing of oxide unicouple thermoelectric modules

Gunstein Skomedal[a*] , Tore Vehus[a], Nikola Kanas[b], Sathya P. Singh[b], Mari-Ann Einarsrud[b], Kjell Wiik[b], Peter Hugh Middleton[a]

[a] *Department of Engineering Sciences, University of Agder (UiA), Jon Lilletunsvei 9, 4879 Grimstad, Norway*
[b] *Department of Materials Science and Engineering, NTNU Trondheim, Norway*

Abstract

Thermoelectric devices based on oxides are good candidates for energy harvesting technologies for use in aggressive conditions where the materials should withstand high temperatures and corrosive environments over prolonged time. This leads to a natural concern for the stability of the electrical contacts, especially on the hot side of the module. In this work, we have assembled several prototype unicouple thermoelectric modules made by pyrolyzed and spark plasma sintered n-type $CaMnO_3$ and p-type $Ca_3Co_4O_9$ and then tested under different conditions mimicking end-user applications. For baseline experiments we have chosen to use nickel as the contact material in order to show the effect of its oxidation on performance. In later work we will utilize more oxidation resistant contact materials. A maximum specific power output of 56 mW/cm^2 with a temperature difference of 760°C was obtained. Cycling test between 400 to 800°C during a period of 1 week showed a reduction in power output of more than 50% mainly due to crack-formation and oxidation near the nickel/oxide interface.

Selection and/or Peer-review under responsibility of 15th European Conference on Thermoelectrics.

Keywords: Thermoelectric oxides; Thermoelectric modules; Stability; Contacting;

* Corresponding author. *E-mail address:* gunstein.skomedal@uia.no

1. Introduction

In the last few years, technologies for harvesting waste heat from industrial and transport sources have gained interest. One such technology is thermoelectric (TE) devices that are assembled in modules to make up complete thermoelectric generators (TEGs) for power generation. In short, TE modules are made from p- and n-type materials, which are connected as *N* number of p-n couples electrically in series and thermally in parallel as seen in Fig. 1. In addition to TE material, a thermoelectric module typically consists of electrical insulating substrates and highly conductive electrodes and contact layers which all will affect the power output. Generally, the electrical resistivity of the electrodes and the contact resistance between electrode and TE material should be minimized, whereas the thermal conductivity of the substrates and electrodes should be maximized.

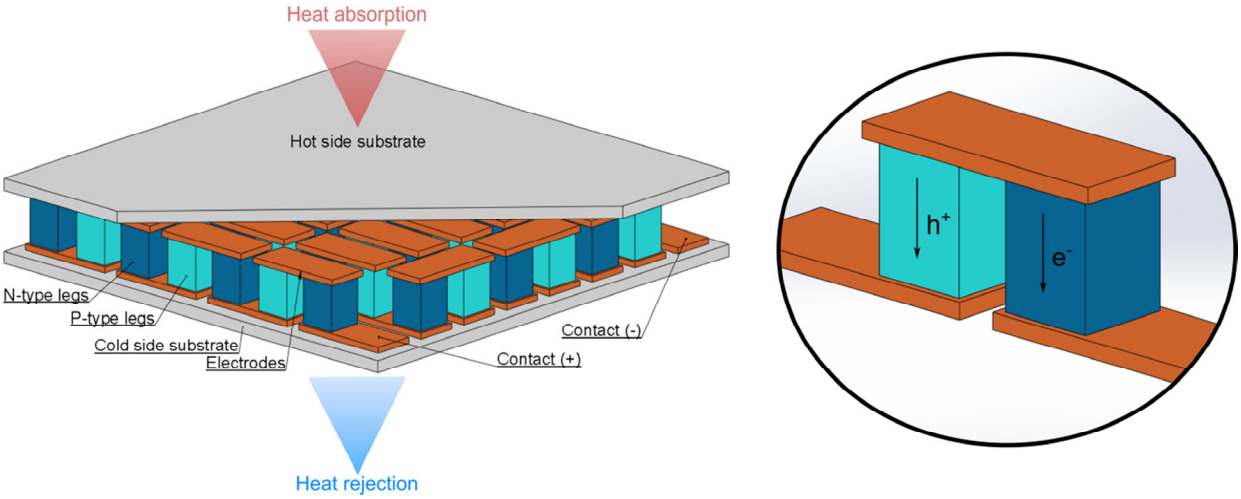

Fig. 1. Schematic Fig. of a thermoelectric module to the left, with a zoom in on to the right of a unicouple of n- and p-type legs including hot and cold side current electrodes. This is the design also used in fabrication of the unicouple test modules in this work.

The total inner electrical resistance, R_i, is given by the sum of resistance from each leg, metallic electrodes and the contact resistances between legs and electrodes, R_c. In most cases the resistance of the electrodes is orders of magnitude less than the total resistance, and can thus be ignored, so that R_i can be expressed as

$$R_i = N\left(\frac{l}{\sigma_p A_p} + \frac{l}{\sigma_n A_n}\right) + R_c \tag{1}$$

where σ_p and σ_n are the electrical conductivity of p- and n-type material respectivly, A_p and A_n are the cross-section area of each leg and l is the leg length. When a thermoelectric module is subjected to a temperature difference, a voltage, V_{OC}, is generated due to the Seebeck effect, which is given by the integral value of the difference in Seebeck coefficient of the p- and n-type, α_p and α_n, between the cold and hot side temperature, T_C and T_H

$$V_{OC} = N\int_{T_C}^{T_H} (\alpha_p - \alpha_n) dT \tag{2}$$

Connecting the module to an external electric load, R_L, it can be shown that the maximum power of the module is found under load matching conditions ($R_L = R_i$) and that it is expressed as

$$P_{max} = \frac{V_{OC}^2}{4R_i} \tag{3}$$

The conversion efficiency of a thermoelectric material is dependent on the material properties given by the dimensionless figure of merit, zT.

$$zT = \frac{\alpha^2 \sigma}{\kappa} T \tag{4}$$

where κ is the thermal conductivity and α and σ are defined as above. Since the thermoelectric properties are temperature dependent, often the average zT in a given temperature range is used. Furthermore, as already explained, the thermal and electrical contact interfaces introduce further losses which reduces the actual conversion efficiency of the module. The average module $Z\bar{T}$ (uppercase ZT is hereafter used for the module, whereas lowercase zT is used for the active thermoelectric materials) is therefore often significantly lower than the respective material zT values. The total conversion efficiency, η, of a module depends on the temperature difference and the average dimensionless figure-of-merit, i.e. $Z\bar{T}$, of the module:

$$\eta_{max} = \frac{T_H - T_C}{T_H} \frac{\sqrt{1 + Z\bar{T}} - 1}{\sqrt{1 + Z\bar{T}} + \frac{T_C}{T_H}} \tag{5}$$

Today's state-of-the-art materials (Bi_2Te_3, PbTe, SiGe) typically contains toxic, expensive and rare elements and are limited to lower temperatures due to decomposition, oxidation or sublimation. Oxide based thermoelectric materials, on the other hand, are capable of operating at high temperatures in air [1]. Even though the zT and the efficiency are much lower in oxides compared to other materials, for many applications, other parameters such as power density (W/cm^2), cost ($/W) and operational lifetime and durability (>10000 hours) are of higher importance. However, operating at higher temperatures puts more demand on the stability of the metallic interconnects leading to degradation and performance issues [2]. It is thus of interest to develop thermoelectric modules and generators based on cheap and abundant oxide materials with stable interconnects that can be produced and processed in a scalable way and withstand high temperature differences and cycling conditions over prolonged time.

There are several good examples from the last 15 years of thermoelectric modules made of only oxide materials [3-10]. Most of these modules were made from calcium cobaltite -$Ca_3Co_4O_9$ (CCO) as p-type material, and either strontium titanate ($SrTiO_3$), zinc oxide (ZnO) or calcium manganite - $CaMnO_3$ (CMO) based compounds as n-type material [11]. A good overview of module dimensions, contacting material and power output can be found in references [7] and [9]. Almost all the modules use a combination of Ag strips and paste for electrode and contacting [12], and there is limited studies considering other more cost effective materials. So far some of the best all-oxide modules have reached a power density (P_{max} divided by total TE area) of 240 mW/cm^2 with a temperature difference up to 785K [5]. Only a few of the modules have been measured over prolonged time periods, but in such cases the reported stability seems to be good. However, all these long-term tests have been carried out under isothermal conditions. Rapid thermal cycles, which would be the case for many real applications, have to our knowledge not been studied.

The main goal of this study has therefore been to investigate low cost and durable solutions for incorporation of oxide materials in a TE module subjected to thermal cycling procedures. It is clear that most of the degradation occurs on the hot side. For our preliminary work we have purposely chosen to use Nickel as the interconnect material because it is chemically compatible with the oxide TE materials, even though it forms a non-conducting oxide film after exposure to air [13]. In later work we will investigate oxidation resistant metals and metal alloys that form a passive but conducting oxide layer.

2. Experimental

Powders of $Ca_3Co_4O_9$ (CCO, p-type), $Ca_{0.931}MnO_3$ (CMO, n-type) were synthesized by spray pyrolysis (CerPoTech AS, Trondheim-Norway). n-type is intentionally Ca deficient and corresponds to a composite of 90 vol% $CaMnO_3$ (perovskite) and 10 vol% $CaMn_2O_4$ (spinel) and was chosen due to improved TE-properties compared with single phase $CaMnO_3$ [14]. Pellets were fabricated by spark plasma sintering (SPS, Dr. Sinter 825), using a 20 mm graphite die under vacuum. Both materials were sintered at 880 °C and 75 MPa for 2 min. Heating and cooling rates were chosen to be as fast as possible and averaging 120 °C/min. The sintering conditions were

chosen so that the CMO legs had a low relative density of 70% (3.2 g/mm^3), whereas the CCO legs had a higher density of 94% (4.4 g/mm^3). The peak power factor ($\alpha^2\sigma$) for CCO was $3.5 \cdot 10^{-4}$ W/(m·K) and $8 \cdot 10^{-5}$ W/(m·K) for CMO, see [15] for details of the TE characterization of these materials. Each pellet was polished down to a height of 3.7 mm with a P2400 grit SiC paper finish. The pellets were then cut into several rectangular legs of 4 x 4 or 4 x 3 mm. Some of the legs were also coated on both hot and cold side with a layer of 50-100 nm gold in a sputtering machine, see Fig. 2.

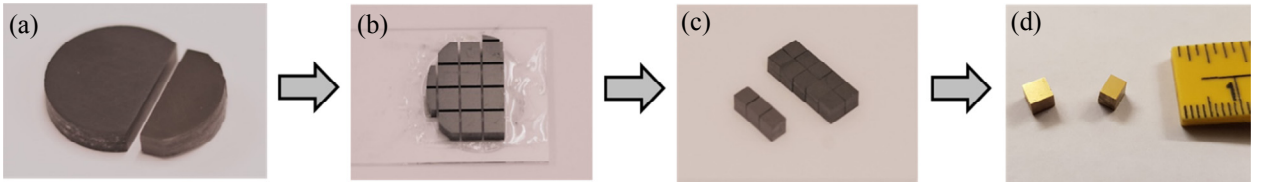

Fig. 2. Leg manufacturing steps. (a) pellet polishing and height adjustment. (b)-(c) leg dicing. (d) metallization

The test set-up is illustrated in Fig. 3a and was built "in-house". The schematic is shown in Fig. 3b. It consists of a cooling block (copper) which was water-cooled, with an external cooler (Minichiller, Huber Kältenmaschinenbau AG, Germany), which was set to 20°C. A recess for a K-type thermocouple was also made in the Cu-block. An Inconel block with a 100W heater (Dalton WattFlex, USA) was used to heat the sample, and was connected to an external power supply (EA-PS 2084-10B, Elektro-Automatik, Germany). The Inconel block had two recesses for K-type thermocouples positioned straight above each leg in the unicouple. Three different unicouple modules were assembled and tested. For electrical contact on the hot side, a 1 mm thick nickel plate was used (Sigma Aldrich), while on the cold side a 0.1 mm silver foil (Sigma Aldrich) was used. These unicouples where then pressed between two alumina (Al_2O_3) plates of 0.25 mm thickness for electrical insulation, with a pressure of approximately 2-2.5 MPa was applied with compression springs. The first module (module 1) used only press-contact between the cold side silver electrode and the hot side nickel electrode. For module 2, additional Ag-paste (Sigma Aldrich) was used on the cold side TE-leg/silver electrode interface to improve cold-side electrical contact, and for module 3 a thin layer of Au was sputtered on both sides of the leg to act as an additional contact layer on both interfaces. A NI DAQ (National instruments) with analog input board were used together with LabView to continuously monitor hot and cold side temperature ($T_{H,n}$, $T_{H,p}$ and T_C) and open circuit voltage (V_{OC}) in additional to controlling the hot side temperature and an active load used for I-V curve scans (3721A 400W electronic load, Array Electronic Co., Nanjing, China). Each module was slowly ramped up in steps of 200°C up to a maximum hot side temperature of 800°C. The modules were then cycled between alternating hot side temperature of 800°C for 1 hour and 400°C for 10 minutes, with approximately 80°C/min heating and cooling rate. For each cycle, the module I-V curve was recorded.

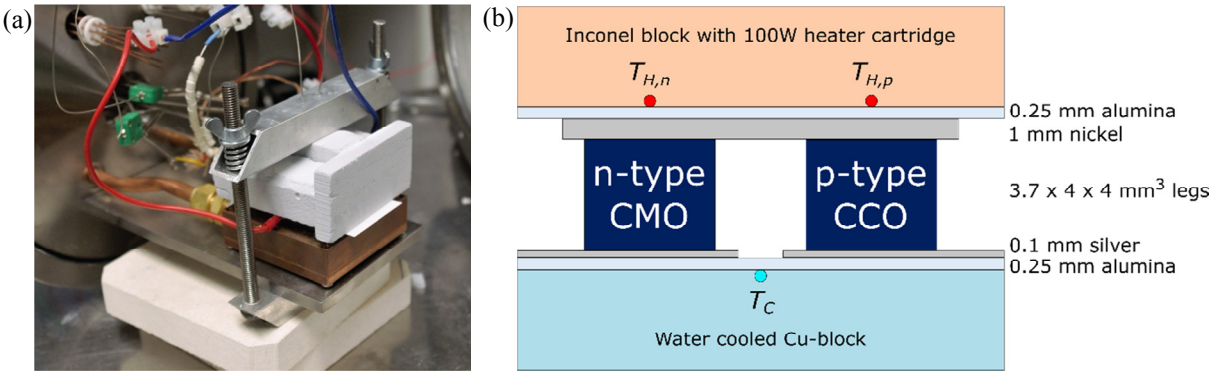

Fig. 3. (a) Picture of test set-up with connections and insulating plate covering the module above the water-cooled Cu-block. (b) Sketch of module cross-section and test assembly with temperature measurement points ($T_{H,n}$, $T_{H,p}$, T_C)

The microstructure and the composition of the cross-section of each module after cycling were examined with scanning electron microscope (SEM, Zeiss Merlin) and energy dispersive X-ray spectrometer (EDS).

3. Results

A total of three thermal cycling testes were carried out, one for each module. All modules showed a V_{OC} close to the expected value calculated from the measured Seebeck coefficient by using equation (2). A deviation of up to 15% is found at the highest temperatures as seen in Fig. 4a. The V_{OC} increased monotonically with increasing hot side temperature as expected, since the cold side water reservoir temperature was kept constant at 20°C. For each temperature, a I-V curve was measured, and the inner resistance and power output of the module calculated, see Fig. 4b. For module 1 and 2, the starting inner resistance, R_i, was very high at low temperatures (>10 Ω), but decreased as the temperature increased and stabilized at the maximum test temperature of 800°C, with the lowest value found for module 3 at 1.2Ω, see Fig. 5a. By inserting the measured electrical conductivity of the two materials into equation (1), the total resistance of these should be close to 0.45 Ω which means that the contact resistance, R_c, should be 0.75 Ω i.e., almost 70% of R_i of module 3. For module 1 and 2 this was even higher. The resulting maximum power, P_{max}, of module 3 was 15.6mW which is equivalent to a power density of 56 mW/cm^2.

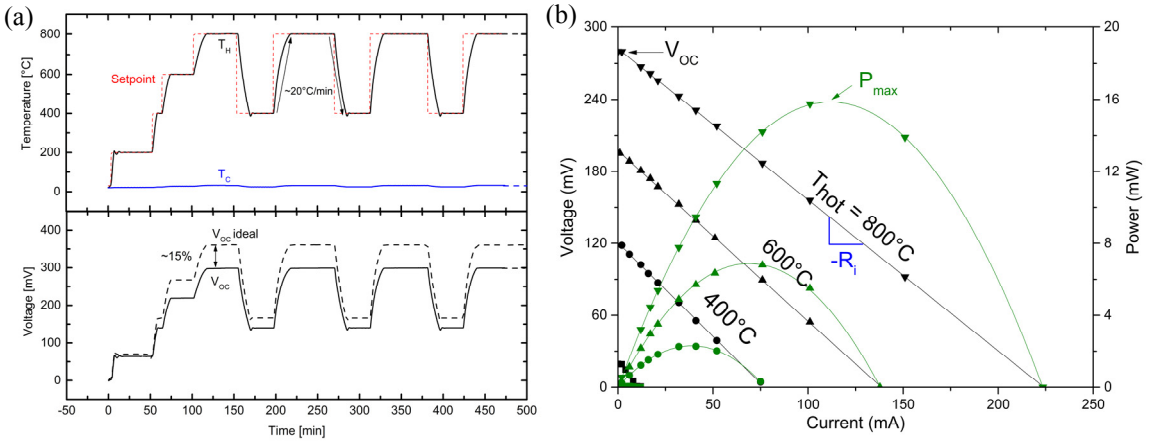

Fig. 4. (a) Module hot and cold side temperature (T_H and T_C) and open circuit voltage (V_{OC}) as a function of test time with increasing hot side temperatures (200-400-600-800°C) for Module 1, and subsequent cycling between 400 and 800°C. (b) I-V curves for Module 3 at different hot side temperatures.

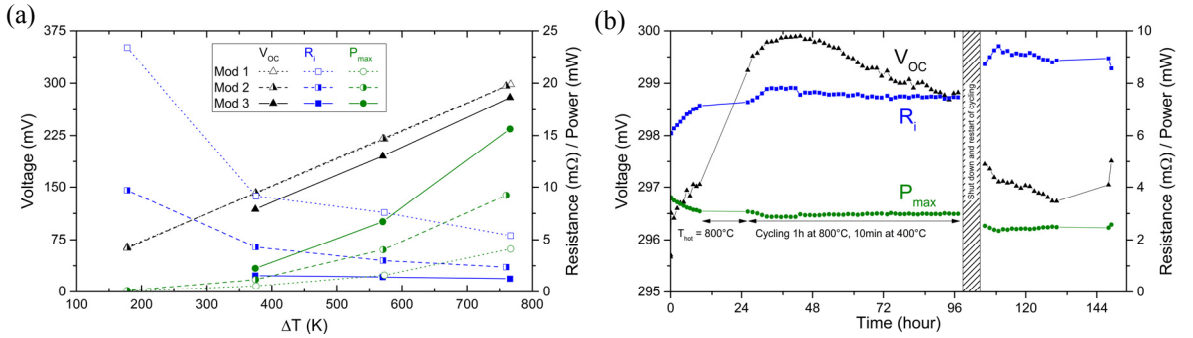

Fig. 5. (a) V_{OC}, R_i and P_{max} as a function of temperature difference ($\Delta T = T_H - T_C$) of the three modules before start of cycling. (b) Evolution of V_{OC}, R_i and P_{max} at T_H = 800°C for module 1.

After ramping up hot side temperature in steps, all three modules were tested in thermal cycles for around 150 hours total. For module 1, the test was also stopped completely and then restarted which had a significant effect on the R_i values of the module as seen in Fig. 5b, increasing up to 20%. Module 1 had an initially high R_i, but

stabilized after around 20 hours of testing, while module 2 and 3 (Fig. 6) showed a gradual increase in R_i over time. The V_{OC} was very stable for all three modules during the whole test-period with only a variation of around 1%. A summary of V_{OC}, R_i and P_{max} for all modules is found in Table 1.

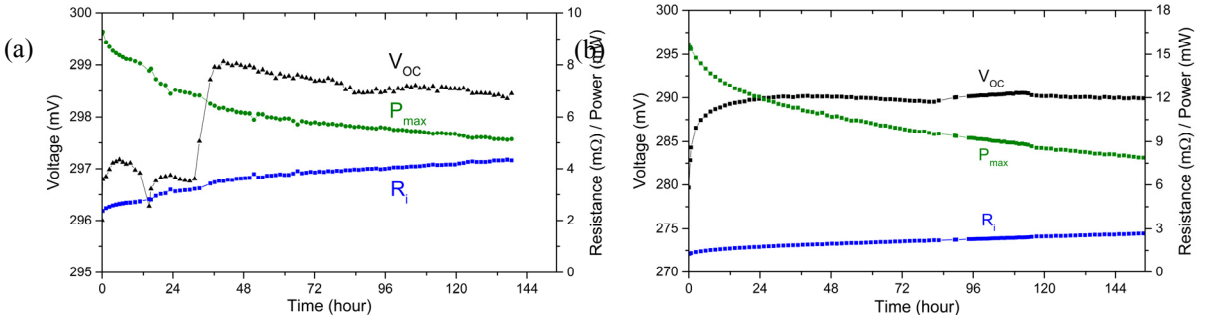

Fig. 6. Evolution of V_{OC}, R_i and P_{max} at T_H = 800°C for module 2 (a) and module 3 (b) during cycling up to 140 and 150 hours respectively

Table 1. Summary of cycling test results. BOT/EOT = beginning/end of test.

Parameter	Unit	Module 1	Module 2	Module 3
V_{OC} (BOT/EOT)	mV	296 / 297	296 / 298	278 / 290
R_i (BOT/EOT)	Ω	6.1 / 8.3	2.4 / 4.3	1.2 / 2.8
P_{max} (BOT/EOT)	mW	3.6 / 2.6	9.3 / 5.1	15.6 / 7.5
Power density (BOT)	mW/cm^2	11.3	29.1	55.7

After cycling, the unicouples were carefully taken out of the test assembly. Since only press-contact was used and the temperature remained below 50°C during testing on the cold-side of the modules (the water-chiller was kept at 20 □, but the measured temperature on the cold side was sometimes higher than the setpoint temperature), no reaction/change was seen either visually or in SEM on the cold-side for any of the modules. The focus of the remainder of the results are therefore limited to hot side interfaces. For module 1 and 2, the n-type CMO leg fell off during disassembly, and clear and sharp cracks could be seen (Fig. 7a). Small parts were also found to be still adhering to the hot side nickel electrode (Fig. 8a). In both these modules, the p-type CCO legs were firmly fastened to the nickel electrode after end of cycling, suggesting good diffusion bonding and little crack formation (Fig. 7b and Fig. 8b). A thin NiO intermediate layer of approximately 4-5 µm was formed after around 150 hours of cycling, or approximately 75 hours at the maximum temperature of 800 °C. This layer seems to adhere very well to the CCO surface, with very sharp and defined interfaces. Similarly, there is also some Ni diffusion into the CMO leg where there is contact, and it seems that NiO is formed within the pores in the CMO.

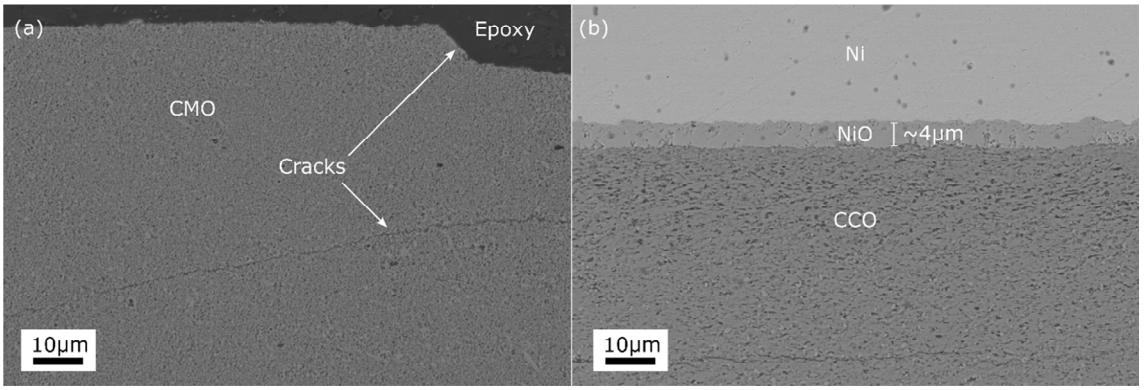

Fig. 7. n- (a) and p-type (b) legs of module 1. CMO legs seen to have cracked off during testing, while CCO adheres well to Ni electrode through an intermediate NiO layer formed during testing.

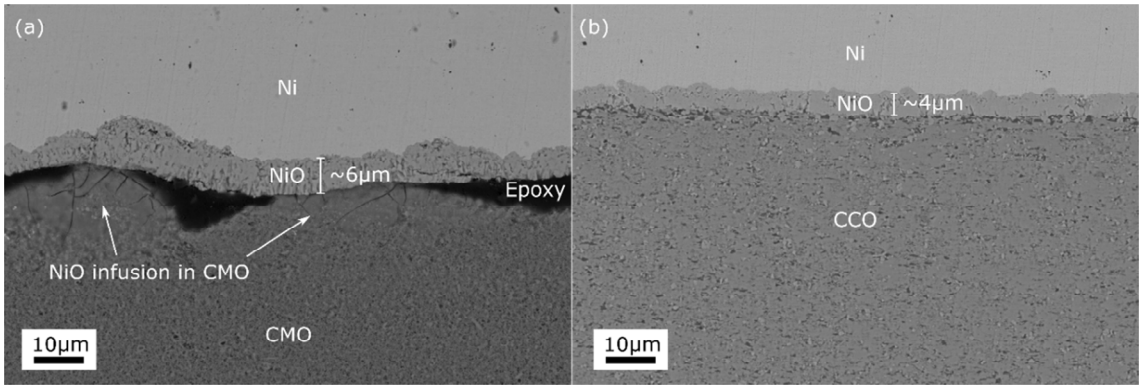

Fig. 8. n- (a) and p-type (b) legs of module 2. Small areas with some diffusion of Ni into CMO. CCO bonds well with Ni through 4µm NiO layer

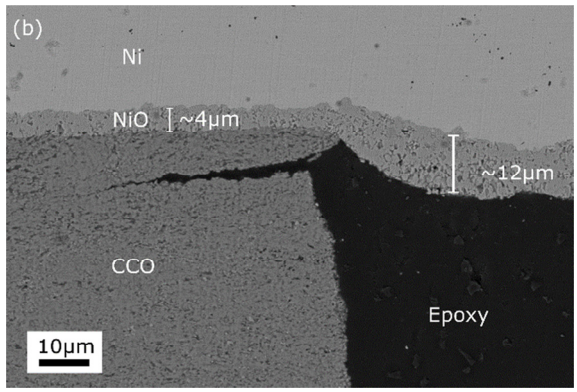

Fig. 9. Edge effect for CCO leg for module 2.

Near the edges of the CCO legs (for both module 1 and 2), slight plastic deformation of the nickel electrode was seen, followed by lateral cracks from the corner along the interface and into the CCO legs (Fig. 9). The NiO layer was around 15 µm on uncovered nickel surfaces not in direct contact with the TE legs, which reflects the native oxidation rate of pure nickel. This aspect will be addressed in future studies using non-nickel based interconnects.

As expected, module 1 and 2 were quite similar in terms of electrical contact, where low electrical contact to CMO was responsible for most of the high R_i. For module 3, with Au-coated legs, the situation was somewhat the opposite, with seemingly good contact for CMO and less good for CCO. As seen in Fig. 10, the CMO adhered very well to the nickel electrode, with two clear intermediate layers visible; NiO and a NiO/CMO mixture, where NiO seems to have infused into the CMO pores. All the Au from the coating has accumulated as small droplets near the Ni/NiO interface. For the CCO leg in module 3 (see Fig. 11), around 1/3 of the CCO/NiO/Ni interface was separated by a gap, pointing to little contact and diffusion bonding of this region. One explanation of this could simply be that slight height variation of the leg caused non-satisfactory contact during initial heating and testing. The Au had accumulated as droplet near the Ni/NiO interface in the regions where the CCO leg was in good contact. However, some Au also remains on the pristine CCO surface, particularly in the non-contact regions.

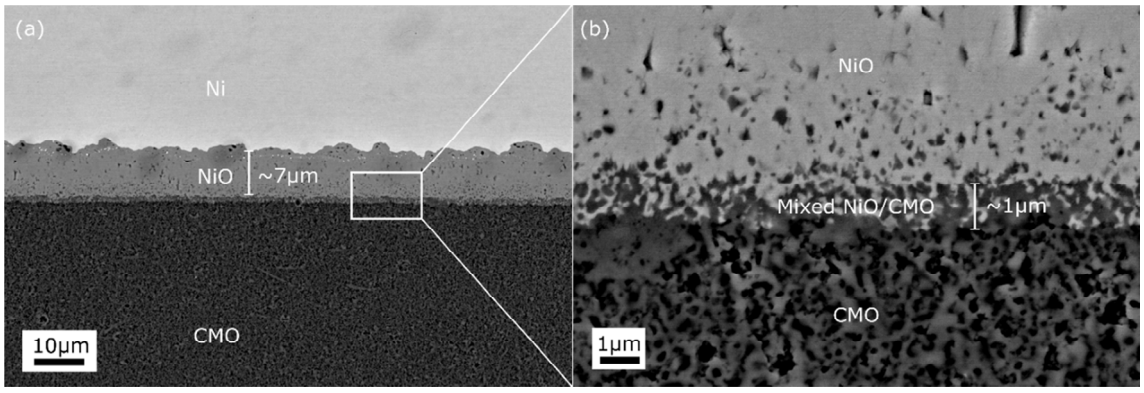

Fig. 10. (a) Interface between CMO and Ni electrode of module 3, showing good bonding between CMO and Ni with intermedia 7 µm NiO layer. (a) A thin (~1µm) mixed NiO/CMO layer is formed between CMO and NiO.

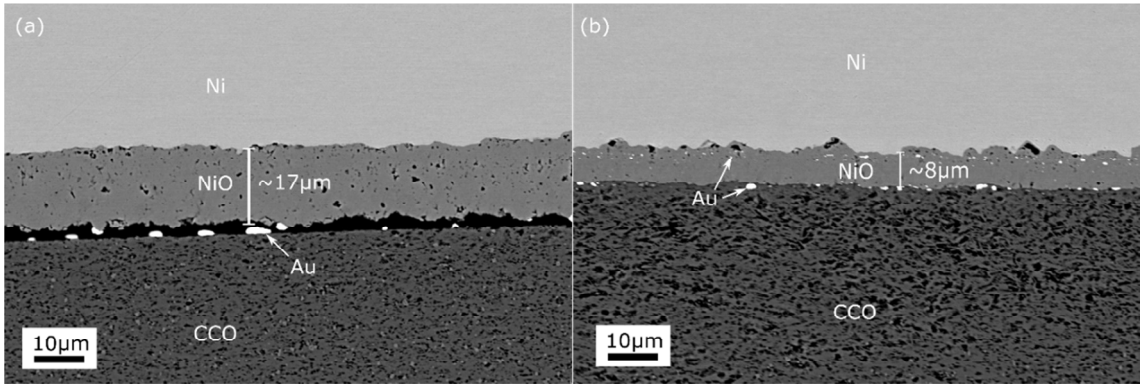

Fig. 11. Pictures taken at two different positions at the interface between CCO and Ni-electrode of module 3. In (a) there has been no bonding during test, while (b) shows area with good bonding. Au accumulated in small droplets both close to CCO surface and at NiO/Ni interface. Signs of formation of voids at Ni/NiO surface for thicker NiO layer.

4. Discussion

Mechanical stability

The designed test set-up provided an easy way to investigate TE and contacting materials during cycling. Even though a simple connection with pressure contact was used for all unicouple modules, high stable temperature difference and reproducible cycling were obtained. Although not used in the present study, the ability to perform high-temperature investigations of TE with the "in-house" made test set-up can provide information into phenomena such as interdiffusion and oxidation mechanisms and kinetics [16]. Man et al. has also made a similar test set-up which enables high-temperature investigations, where mechanical pressure is included, and for their applications a pressure of 1.3 MPa was considered optimal in terms of conductivity [17]. However, the caveat in applying more pressure is the higher risk of increased cracking of the test legs.

As seen in many of the SEM images of the cross section near the hot side, crack formation was clearly an important problem explaining much of the increase in internal resistance during cycling, particularly for the CMO legs of module 1 and 2. This has mainly two causes. First, CMO and nickel clearly do not form a good and stable interdiffusion layer (except for module 3 where Au seems to help,). Secondly, mechanical stresses formed under high thermal gradients causes crack formation and breakage of the thermoelectric material. Mechanical stress is further exacerbated by different coefficients of thermal expansion of the materials. NiO has a relative linear thermal expansion ranging from 12 to 15 ppm/K [18], and Ni has approximately 13 ppm/K, CCO 14.4-17 ppm/K and CMO 18 ppm/K [19, 20]. In addition, the respective materials Young's modulus will dictate the mechanical

response to the induced stresses, causing the more brittle material to crack while the more elastic material will deform. This effect is seen in the example of Fig. 9, showing the cracked edge of the thermoelectric legs on the hot side, while the nickel and adhering oxide layer has plastically deformed and contains no cracks. The lateral cracks in the thermoelectric legs will increase the inner resistance of the module over time as the cracks propagate.

Even though only pressure contacts are made between Ni and CCO, a satisfactory electrical contact was made, especially as the temperature was increased eventually leading to diffusion bonding (see Fig. 5). However, for CMO in module 1 and 2, the interface was not homogeneous (see Fig. 7a and Fig. 8a), which implies that the plasticity of CMO was less than for CCO where cracking was observed. A study by Kenfaui et al. on $Ca_3Co_4O_9$ showed that the SPS parameters, especially pressure and temperature applied during the SPS process, affected the hardness, Youngs' Modulus, strength and fracture process [21]. When gold was used in our study, the CMO appeared more stable, which implies that Au contribute to increased plasticity, although it appears as gold agglomerate only at the interface between NiO and Ni. Further studies into the CCO and CMO material is needed to quantify the mechanical stability influence by contacting materials.

Contact resistance reduction with Ag, Au and Ni

For all modules, a uniformly thick NiO layer ranging from 4 – 17 μm formed between the TE leg and the nickel electrode. This layer contributed significantly to efficiency loss in TE modules, by increasing the electrical contact resistance and thus inner resistance of the module. Over time, as the oxide layer slowly thickened and it can be assumed that the contact resistance increased approximately linearly with oxide thickness. On average, NiO had 100 to 1000 times higher electrical resistance compared to pure metallic Ni [18]. Oxidation of Ni is a solid state diffusion controlled process following parabolic kinetics [13], and it is evident that oxidation will progress with time, making Ni unsuitable for contacting high-temperature TE in oxygen-rich environment. However, in a real device, the partial pressure of oxygen will be dramatically reduced inside the modules (due to hermetic packaging) at the interface between thermoelectric material and Ni, the oxide layer will gradually stop growing and should eventually stabilize to an acceptable level. The diffusion mechanisms for the growing NiO layer will not be furthered discussed here since Ni would not be the preferred choice for contact material. As emphasized at the beginning of this article, we chose nickel as a baseline material to compare more favorable candidates in a later study.

For module 3, the lowest resistance was obtained of around 1.2Ω, but the contact resistance was still >50% of total resistance, whereas it should be in the range of 1-10%. An initial Au layer seemed to reduce the resistance somewhat. The reason for the improved diffusion contact between CMO and nickel with an Au contact layer is uncertain, and should be investigated further since it offers an interesting option for adapting oxide thermoelectric materials into classical modules with metallic contacts without the use of expensive electrode materials such as silver.

Even though silver is a common state-of-the art contacting material and electrode for oxide-based thermoelectric modules, silver is not a necessarily a cost-effective material choice for large scale applications. Other materials providing a stable thin intermediate layer would be beneficial. This requires carefully tuned mechanical properties (matching of CTE and Youngs' modulus) and low contact resistance by introduction of thin, stable and highly conductive interdiffusion layer with capacity to act both as contact and anti-diffusion layer. Additionally, *in-situ* formed contacting on the hot side is desirable, as it could ease the industrial production and manufacturing. Hence, further studies should be focused on finding contact materials and processes that fulfill the above-mentioned criteria.

5. Conclusion

In this study, a test set-up has been designed, constructed and used to investigate long-term stability of TEGs based on CCO and CMO. The test rig provided stable cold side temperatures and is able to provide sufficient heat to achieve a hot side temperature up to 800°C and also enable long-term cycling. Although not included here, it is also designed to operate in different atmospheres. The assembled module, provided a maximum power output of 16 mW at ΔT of 765 K, and the presented and discussed data show that the CCO and CMO materials are stable even after

prolonged cycling with from 400 – 800°C. Future work will investigate the development of low cost and durable contact materials compatible with CCO and CMO.

Acknowledgements

We acknowledge financial support from the Research Council of Norway (Project No. 228854)

References

1. Fergus, J.W., *Oxide materials for high temperature thermoelectric energy conversion.* J. Eur. Ceram. Soc., 2012. **32**(3): p. 525-540.
2. Skomedal, G., *Thermal durability of novel thermoelectric materials for waste heat recovery*. 2016, University of Agder: Kristiansand, Norway.
3. Matsubara, I., et al., *Fabrication of an all-oxide thermoelectric power generator.* Appl Phys Lett, 2001. **78**(23): p. 3627-3629.
4. Funahashi, R., et al., *Ca2.7Bi0.3Co4O9 ／La0.9Bi0.1NiO3 thermoelectric deviceswith high output power density.* Appl Phys Lett, 2004. **85**(6): p. 1036-1038.
5. Populoh, S., et al., *Construction of a high temperature TEG measurement system for the evaluation of thermoelectric oxide modules.* Funct. Mater. Lett., 2013. **06**(05): p. 1340012.
6. Funahashi, R., et al., *A portable thermoelectric-power-generating module composed of oxide devices.* J. Appl. Phys., 2006. **99**(6): p. 066117.
7. Van, N.N. and N. Pryds, *Nanostructured oxide materials and modules for high-temperature power generation from waste heat.* Adv. Nat. Sci.: Nanosci. Nanotechnol., 2013. **4**(2): p. 023002.
8. Feldhoff, A. and B. Geppert, *A High-Temperature Thermoelectric Generator Based on Oxides.* Energy Harvesting and Systems, 2014. **1**(1-2): p. 69.
9. Hung, L.T., et al., *Segmented Thermoelectric Oxide‐Based Module for High‐Temperature Waste Heat Harvesting.* Energy Technol., 2015. **3**(11): p. 1143-1151.
10. Bittner, M., et al., *Oxide-Based Thermoelectric Generator for High-Temperature Application Using p-Type Ca3Co4O9 and n-Type In1.95Sn0.05O3 Legs.* Energy Harvesting and Systems, 2016. **3**(3): p. 213.
11. Yin, Y., B. Tudu, and A. Tiwari, *Recent advances in oxide thermoelectric materials and modules.* Vacuum, 2017.
12. Lim, C.-H., et al., *A study of electrodes for thermoelectric oxides.* Electron. Mater. Lett., 2013. **9**(4): p. 445-449.
13. Haugsrud, R., *On the high-temperature oxidation of nickel.* Corros. Sci., 2003. **45**(1): p. 211-235.
14. Singh, S.P., *PhD thesis*. 2018, NTNU: Trondheim, Norway.
15. Kanas, N., et al., *All-oxide thermoelectric module with in-situ formed non-rectifying complex p-p-n junction and transverse thermoelectric effect.* ACS Appl. Mater. Int (submitted), 2018.
16. Skomedal, G., et al., *Evaluation of Thermoelectric Performance and Durability of Functionalized Skutterudite Legs.* J. Electron. Mater., 2017. **46**(4): p. 2438-2450.
17. Man, E., et al., *A High Temperature Experimental Characterization Procedure for Oxide-Based Thermoelectric Generator Modules under Transient Conditions.* Energies, 2015. **8**(11): p. 12341.
18. Keem, J. and J. Honig, *Selected electrical and thermal properties of undoped nickel oxide*. 1978: Defense Technical Information Center.
19. Mazur, N.M., *Microstructural design of CaMnO3 and its thermoelectric proprieties*. 2015, NTNU.
20. Mishra, S., et al., *Spin-phonon coupling and high-pressure phase transitions of R Mn O 3 (R= Ca and Pr): An inelastic neutron scattering and first-principles study.* Phys. Rev. B, 2016. **93**(21): p. 214306.
21. Kenfaui, D., et al., *Ca3Co4O9 ceramics consolidated by SPS process: Optimisation of mechanical and thermoelectric properties.* Mater. Res. Bull., 2010. **45**(9): p. 1240-1249.